

LASER INTERFEROMETER GRAVITATIONAL WAVE OBSERVATORY
- LIGO -
CALIFORNIA INSTITUTE OF TECHNOLOGY
MASSACHUSETTS INSTITUTE OF TECHNOLOGY

Document Type LIGO-T010076-01 - D 7/1/2001
Optical Layout for Advanced LIGO
D. Coyne

Distribution of this draft:

LIGO Scientific Collaboration

This is an internal working note
of the LIGO Project.

California Institute of Technology
LIGO Project - MS 51-33
Pasadena CA 91125
Phone (818) 395-2129
Fax (818) 304-9834
E-mail: info@ligo.caltech.edu

LIGO Hanford Observatory
P.O. Box 1970, Mail Stop S9-02
Route 10, Mile Marker 2
Richland, LA 99352
Phone (509) 372-8300
Fax (509) 372-8137

Massachusetts Institute of Technology
LIGO Project - MS 20B-145
Cambridge, MA 01239
Phone (617) 253-4824
Fax (617) 253-7014
E-mail: info@ligo.mit.edu

LIGO Livingston Observatory
P.O. Box 940
19100 LIGO Lane
Livingston, LA 70754
Phone (225) 686-3100
Fax (225) 686-7189

WWW: <http://www.ligo.caltech.edu/>

Keywords: advanced LIGO, optical layout, core optics, wedge, ghost beams, pickoff beams, cavity lengths

1 OVERVIEW

The advanced LIGO optical system is comprised of the following primary elements:

- (1) the Input Optics (IO)¹, which consist of the modulation, input mode cleaning and input mode matching optics
- (2) the Core Optics Components (COC), which consist of the suspended optics which form the Power recycling Cavity (PRC), the Signal Recycling Cavity (SRC) and the Fabry-Perot (FP) arm cavities,
- (3) the Auxiliary Optics Subsystem (AOS), which consist of the stray light control and beam reducing optics, and
- (4) the Output Optics (OO), which consist of the output mode cleaning optics.

The purpose of this document is to define the fundamental cavity lengths, modulation frequencies and the location of the Core Optics Components (COC); The balance of the optical layout details are then determined by the appropriate subsystems. The overall layout is coordinated through an integrated optomechanical layout drawing which is the responsibility of the systems group.

The core optics components consist of the Power Recycling Mirror (PRM), Signal Recycling Mirror (SRM), Beamsplitter (BS), Folding Mirrors (FM, for the folded interferometer only), Input Test Masses (ITM) and End Test Masses (ETM). These optics generally all have wedged surfaces to deflect ghost beams (due to internal reflections) off of the primary ray path so that they don't interfere with the main beam. In addition, the first reflections off of the anti-reflection (AR) coated surfaces of the ITM and the BS *can* be used as pickoff beams for alignment sensing.

The equations for setting the cavity lengths are defined. The basic criteria for setting the wedge angles, the methods by which they are calculated and the resulting values are given below.

The intent is to maintain this document so that it is current and to eliminate assumptions or inconsistencies with the overall design as the definition of advanced LIGO progresses. In addition to this document the integrated optomechanical layout will also serve this purpose at the detailed level.

2 CAVITY LENGTHS

Based on interferometer sensing analyses^{2,3}, the selected modulation frequencies for advanced LIGO are ~9.0 MHz and ~180.0 MHz. The recycling cavity Schnupp asymmetry was also defined from these sensitivity studies to be nominally 20 cm (added to one arm, subtracted from the other).

-
1. Guido Mueller, David Reitze, et. al., Reference Design Document for the Advanced LIGO Input Optics, LIGO-T010002-00
 2. Ken Strain, "Advanced Interferometer Configurations (AIC): Summary & Recommendations", LIGO Science Collaboration Meeting, Aug., 2000, LIGO-G000280-00.
 3. P. Fritschel, "Advanced LIGO Systems Design", LIGO-T010075-00

2.1. Nominal Parameters

2.1.1. Arm Cavity Length

The center-to-center distance between the LIGO chambers which support the Fabry-Perot arm cavities, in the two longer, unfolded interferometers, is 3995420 mm. The arm cavity length is this dimension plus or minus any positional offset introduced by accommodating the recycling cavity length.

2.1.2. Mode Cleaner (MC) Cavity

The MC free-spectral range (fsr) is ~ 9.0 MHz, thus the MC length = $c/2/\text{fsr} = \sim 16.655$ m. The center-to-center separation between the first and third HAM chambers in the LIGO vacuum system (HAM1 - HAM3) is 16.35 m. Consequently with ~ 30 cm allowance for the short leg of the MC triangle, the MC optics will be very close to the center of the HAM chambers (along the beam direction).

2.1.3. Power recycling cavity (PRC)

The PRC fsr should be equal to $2 \times \sim 9 \text{ MHz} = \sim 18$ MHz. Consequently the PRC length = $c/2/18$ MHz = ~ 8.33 m. Thus PRM to one ITM must be ~ 8.53 m and to the other ITM must be ~ 8.13 m. Since the center-center separation of HAM3 to BSC3 (the beam splitter chamber) is 8.47 m, we should be able to put PRM within ~ 20 cm of the center of HAM3.

2.1.4. Signal recycling cavity (SRC)

The length of the SRC is given as follows:

$$L_{src} = p \left(\frac{c}{2f_{src}} \right) + \left(\frac{c}{4\pi f_{src}} \right) \delta_{\phi} = 0.8328n - 0.1325\delta_{\phi}$$

where p is an integer, $f_{src} \approx 180 \text{ MHz}$, and δ_{ϕ} is the signal recycling detuning; δ_{ϕ} is typically 0.1, so the length correction factor is only ~ 1 cm.

For $n = 10$, $L_{src} = \sim 8.32$ m, and so the signal recycling mirror could be located close to the center of the HAM4 chamber, depending on where the ITMs end up being located.¹

2.2. Final Cavity Parameters

2.2.1. Non-folded Interferometers

Iterating on the above nominal parameters in order to place the optics close to center on the optics tables within the vacuum chambers, results in the following cavity lengths and modulation fre-

1. The HAM5 chamber may also be a possibility, but it looks tighter: The adjacent HAM chamber separation is 2.6 m, giving the average ITM to HAM5 center distance close to $8.47 + 2.6 = 11.1$ m. For $n = 14$, $L_{src} = 11.64$ m.

quencies, for the unfolded interferometers:

$$L_{arm} = 3995200mm$$

$$L_{mc} = \frac{nL_{arm}}{\left(m + \frac{1}{2}\right)} = 16681mm \text{ for } n = 1 \text{ and } m = 239$$

$$f_{mc} = \frac{c}{2L_{mc}} = 8,985,820Hz$$

$$L_{prc} = \frac{\left(k + \frac{1}{2}\right)L_{mc}}{n} = 8341mm \text{ for } k = 0$$

$$f_{src} = qf_{mc} = 179,716,394Hz \text{ for } q = 20$$

$$L_{src} = p\left(\frac{c}{2f_{src}}\right) + \left(\frac{c}{4\pi f_{src}}\right)\delta_{\phi} = 834p - 133\delta_{\phi} = 8327mm \text{ for } p = 10 \text{ and } \delta_{\phi} = -0.1 \text{ rad}$$

2.2.2. Folded Interferometer

To Be Determined (TBD)

3 LAYOUT TOPOLOGY

The folded and unfolded interferometers share the same beam tube aperture, by being displaced horizontally relative to the vertical centerline. The heights are set to be the same in the Fabry-Perot cavities and in the input optics section for commonality of seismic isolation table heights and suspension structure lengths. The basic topology of the optical layout is depicted in the Figure 1.

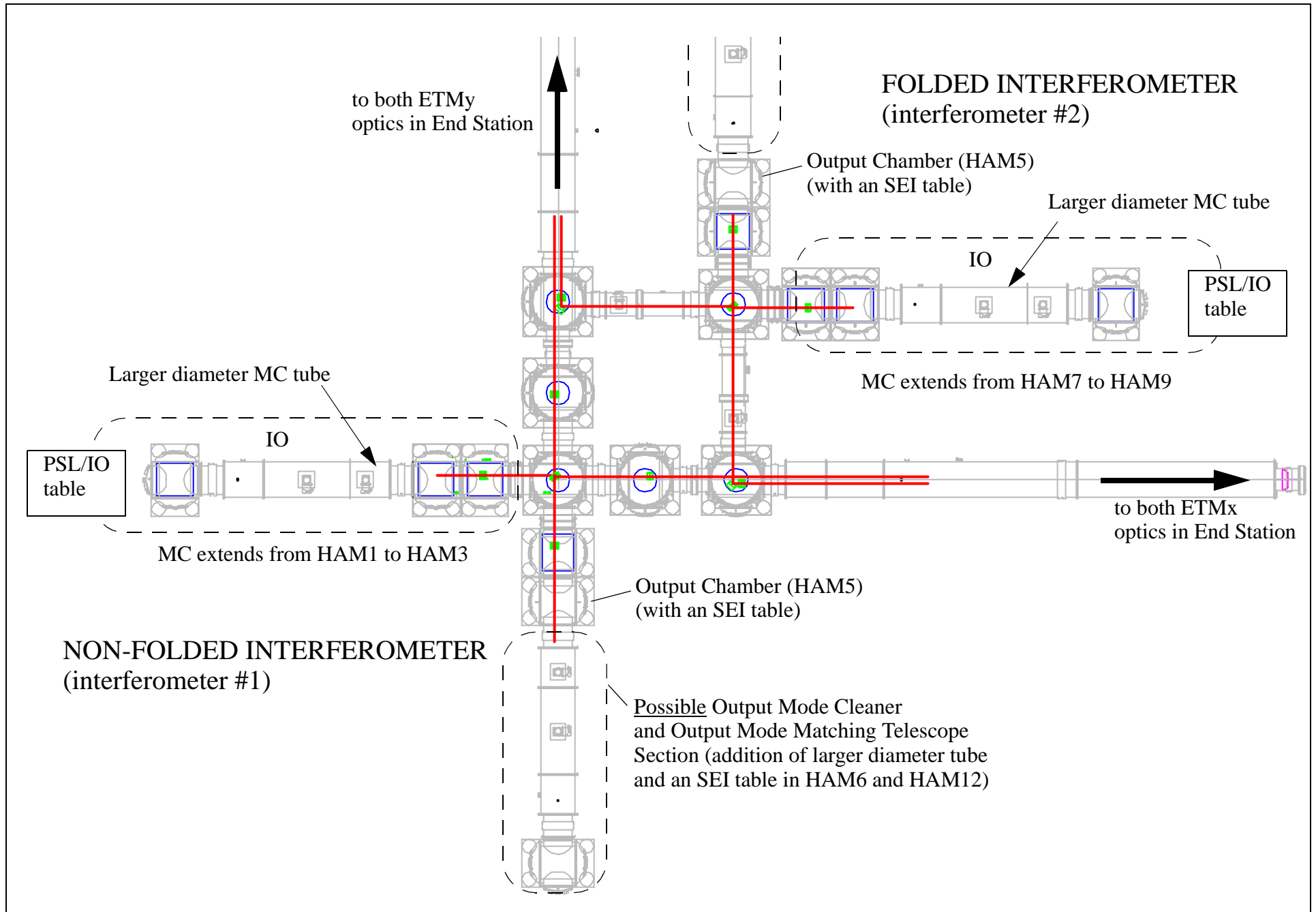
4 LAYOUT CONSTRAINTS & CRITERIA

In addition to the cavity lengths given above and, of course, the LIGO vacuum equipment geometry¹ (with the exception noted below), the following constraints and criteria apply to the optical layout:

1) Lateral separation between interferometer beams: Since the folded interferometer shares the same beam tube as the unfolded interferometer, the beams must be laterally separated enough so that the suspension structures of the input and end test masses of the folded interferometer don't clip the beam of the unfolded interferometer. For 40 kg sapphire masses, the diameter is ~320 mm. Clearance required for the suspension structure is ~80 mm (one sided). The 1 ppm radius associated with the Fabry-Perot cavity beams is ~158 mm (for a 6cm beam waist on the test masses). Consequently the lateral separation of two interferometer beams should be about

1. The LIGO vacuum equipment layout is defined in the following drawings: For the Hanford Observatory: D961165, D961168, D961169, D961170 and D961171. For the Livingston Observatory: D970383, D970384 and D970385.

Figure (1) Basic Optical Layout Topology



$320/2+80+158 = 398$ mm or placed at ± 200 mm from the beam tube centerline (the same as in LIGO-1).

2) The maximum wedge angles, from manufacturing considerations for high precision optics, are as follows:

BS	$1^\circ 0'$ maximum
ITM, PRM, SRM	$3^\circ 0'$ maximum

3) The wedge angle tolerance¹ is $\pm 1'$.

4) Beam Line Height in the HAM Chamber: The limited height above the optics table in the HAM chambers places a significant constraint on the height of the suspension assemblies, particularly for the PRM and SRM. As a consequence it is best to place the optics tables, and the beam line, as low as possible. The constraints on the HAM optics table height and the resulting allowable headroom as a function of position on the table are documented elsewhere². The apparent lower limit of the HAM optics table in LIGO global coordinates is $z = -315$ mm (corresponding to maximum ‘compression’ of the seismic isolation system without serious design consideration). Given that the PRM and SRM diameters³ are 265 mm and assuming a 25 mm clearance from the lower edge of the optic and the optic table, then the minimum laser beam height at the SRM and PRM is $z = -315 + 265/2 + 25 = -157$ mm.

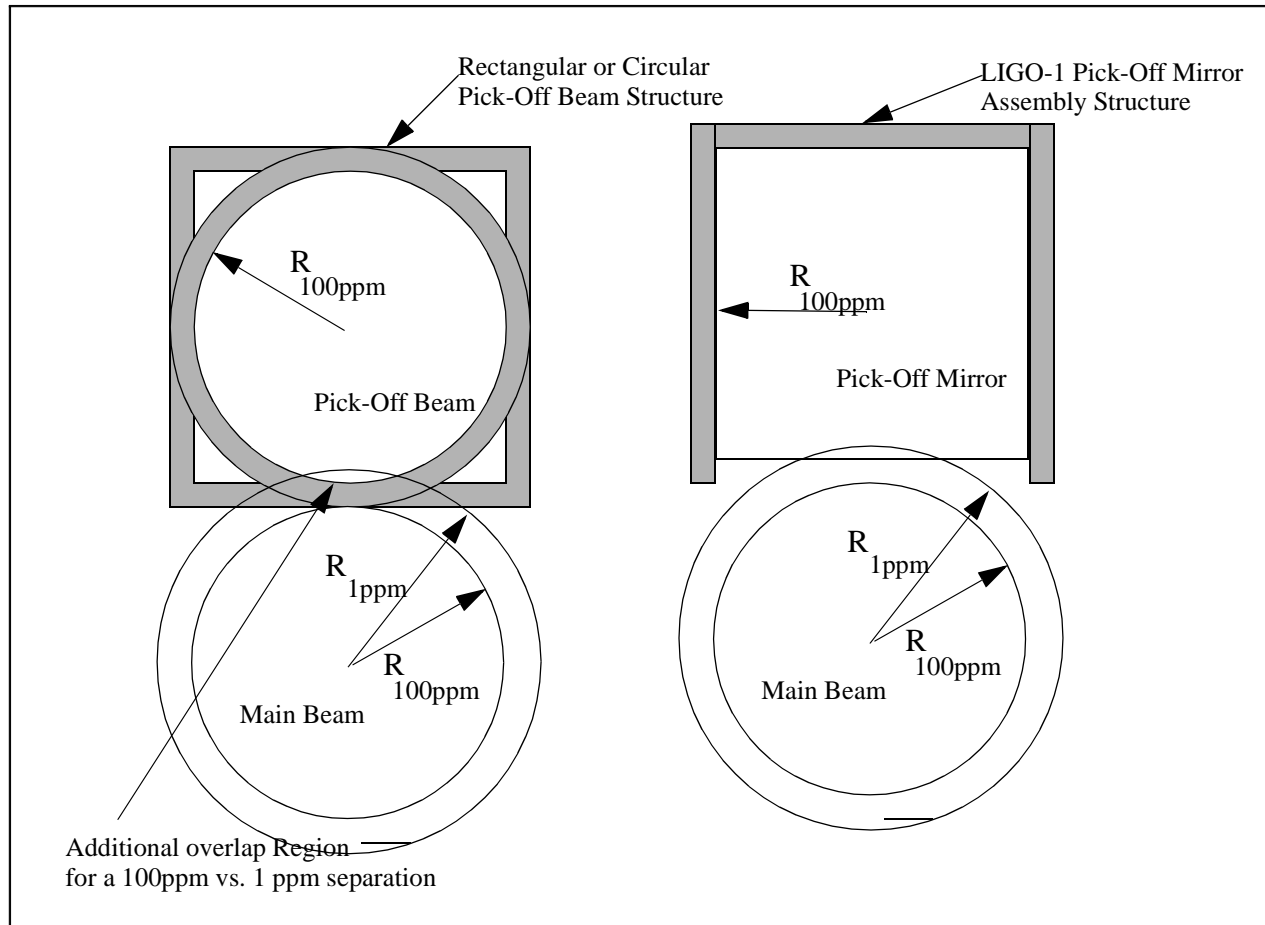
The maximum length, in the axial direction, of the table area available for PRM and SRM suspension placement, with the HAM table at this height is about 915 mm (Function W_x from Table 4 of LIGO-T000087-01) for a suspension structure height of 940 mm (best current estimate of the triple pendulum height).

Physical limits on the height of the optics table in the BSC chamber do not constrain the optical layout.

5) Recycling Cavity Pick-off Beams: The first reflections off of the anti-reflection (AR) coated surfaces of the Beamsplitter (BS) and the Input Test Masses (ITM) *may* be used as pickoff beams for alignment and length sensing and control. These beams must be separated sufficiently to ensure that scattered light from the reflected beam does not contribute significantly to the interferometer noise. In LIGO-1⁴, the primary beam (at the 1 ppm radius) was required to be separated from the pickoff beam (at the 100 ppm radius) by a distance (≥ 50 mm) sufficient to accommodate a beam reducing telescope structure and pick-off mirror cell structure. For advanced LIGO, separating the beams this much is difficult. Since this overlap in the pickoff beam and the main beam occurs only over a small region (see Figure 2), the total loss is small, and setting the separation at the 100ppm radius may be sufficient; This requires further analysis.

-
1. The wedge angle tolerance in LIGO-1 was $\pm 5'$, but far better accuracy was achieved. A smaller tolerance is in fact desirable. The specification here is subject to further review.
 2. D. Coyne, “Available Height above the HAM Optics Table”, LIGO-T000087-01.
 3. P. Fritschel, “Advanced LIGO Systems Design”, LIGO-T010075-00
 4. For LIGO-1 the ITM diameter (25 cm) was selected at the 1ppm level (plus centering tolerance) in order to limit TEM₀₀ mode diffraction loss to acceptable levels. Since the AR coating reflectance is < 0.01 , this criteria implies that the primary beam (at the 1 ppm radius) be separated from the pickoff beam (at the 100 ppm radius) by a distance sufficient to accommodate a beam reducing telescope structure.

Figure (2) Main and Pick-Off Beam overlap



In addition, the LIGO-1 pick-off mirror structure required only 16 mm, not the 50 mm set in the original requirements. I propose 30 mm as a workable value for this parameter.

The Gaussian beam waist in the RC is ~ 60 mm, so that the corresponding 100ppm radius is 129 mm (the 1ppm radius is 158 mm). The required separation is then $2 \cdot 129 + 30 = 288$ mm. This beam separation must occur in the length between isolated tables.

6) Ghost Beam Separation: Similarly, the first ghost beams from each optic must be separated sufficiently from the next optic to allow for structures to beam dump or baffle the beam.

7) Backscatter Limit: An analysis of the beam tube baffle backscatter and diffraction¹ limits the minimum distance of the laser beam center to the edge of the baffles to 200 mm for a 2x increase in the backscatter phase noise (from the case of a centered beam). At ± 200 mm lateral separation, the backscatter limit of vertical position in the LIGO global coordinate system is $z = \pm 275$ mm.

8) Vertical Seismic and Thermal Displacement Noise Coupling: The orientation of the COC surfaces with respect to the local gravity vector causes a coupling of seismic and thermal vertical motion to length motion. The noise due to this coupling for the Power Recycling Cavity (PRC) and Signal Recycling Cavity (SRC) surfaces should be much smaller than the contribution due to

1. Kip Thorne, Eanna Flanagan, beam tube baffle backscatter and diffraction analysis, LIGO-T950132;

the Fabry-Perot (FP) cavity surfaces. The allowable contribution to the noise floor for each RC surface was set at 1/10 of the contribution due to each FP surface (see Appendix 1). In general, since the isolation of the PRM and SRM is less than for the ITMs, an optical layout that minimizes the beam's deviation from horizontal at the PRM and SRM is preferred.

9) Symmetric Wedges: The BS, ITM and RM optics are symmetrically wedged, i.e. each surface is set at one-half the wedge angle relative to the cylindrical axis of the optic. This prevents an internal retro-reflection from a 90° interface between a face and the cylindrical surface.

10) Single Wedges: The ETM and FM optics are single surface wedged. The wedge angle for the ETM and FM are defined as 30'. (The wedge angles for the ETM and FM are not critical since these optics are essentially not used in transmission.)

11) Input and Output Beams Level: The principal ray of the laser light entering the PRM and exiting the SRM should be parallel to the plane defined by the BT axes (i.e. parallel to the LIGO global x-y plane).

12) Common BS Wedge Angle: The wedge angle for the Beamsplitter (BS) for the folded and the unfolded interferometers should be the same.

13) Common PRM Wedge Angle: The wedge angle for the Power Recycling Mirror (PRM) for the folded and the unfolded interferometers should be the same. This is made possible by using the angular alignment degrees of freedom of the Fold Mirrors (FM) in the folded interferometer.

5 LAYOUT ASSUMPTIONS & LIMITATIONS

Known deficiencies, limitations, assumptions or possible changes are listed below.

- 1) The thermal compensation system may require the addition of one or two phase plates in the recycling cavity, as indicated in Figure 3. This has not been included in the optical layout to date.
- 2) The high reflectance (HR) faces of both the PRM and SRM are on the PRC and SRC cavity sides, in the baseline layout. It may be advantageous to reverse the PRM and put the anti-reflection (AR) side of the PRM into the PRC in order to use an active thermal compensation system to correct the common mode component of the thermally induced distortion.
- 3) The material and thickness of each of the core optics is used in the optical layout for optical path length calculation. If material choices and aspect ratios change the optical layout will only be slightly perturbed. The materials and thicknesses used in this analysis are given in the following table:
- 4) The optical layout of the folded interferometer is yet to be done.
- 5) In LIGO-1, three separate recycling cavity pick-off beams have been provided by stipulating large wedge angles on the ITMs and BS in order to separate the first reflections from the AR surfaces. A single recycling cavity pick-off beam seems to be sufficient for observability. For possible cavity locking convenience, and as a worst case scenario (for bounce mode to length coupling), all three beams have also been provided in the advanced LIGO optical layout. The possibility, and advisability, of (a) using a single recycling cavity pick-off beam and (b) of using non-wedged ITMs is under review.

Figure (3) Phase Plates for Thermal Compensation Actuation

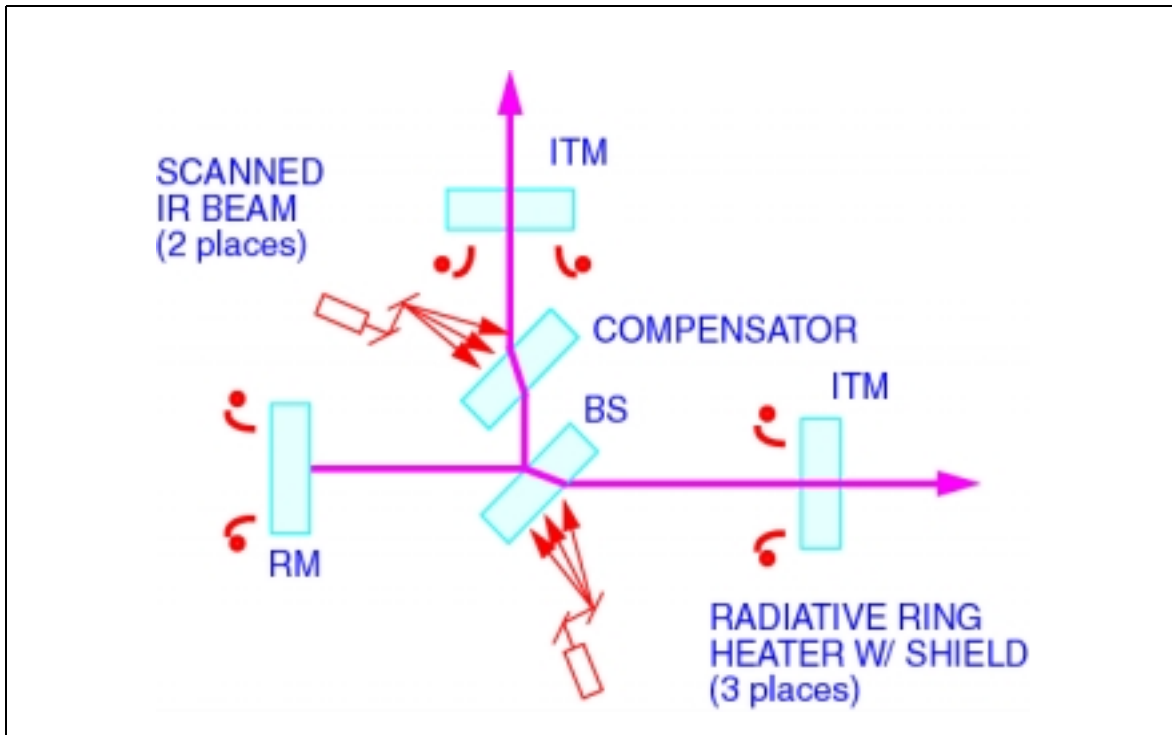


Table 1. Assumed Optic Materials and Thicknesses for Refractive Optics used in the Ray Trace Analysis^a

<i>Optic</i>	<i>Material</i>	<i>Thickness^b (mm)</i>
ITM	sapphire	118
BS	fused silica	60
PRM	fused silica	100
SRM	fused silica	100

- a. Thicknesses are assumed to apply at the thickest part of the wedge for the ITM, PRM and SRM and at the thinnest part of the wedge for the BS (as is the definition for LIGO-1).
- b. N.B.: These thicknesses have changed in the baseline design. The optical layout is only weakly effected by the optic thicknesses.

6 COORDINATE SYSTEM

The LIGO global coordinate system¹ is defined with its coordinate axes aligned along the center

1. A. Lazzarini, Determination of the as-built LIGO Global Coordinate Axes for Hanford, WA: Final analysis of the LIGO BT/VE interface survey monuments”, LIGO-T960176-C-E, 26 Nov. 96.; This supersedes “Orientation of the Beam Tube Enclosure Foundation with Respect to the Local Horizontal: Hanford Site, LIGO-D950140-A, 28/11/95, which needs to be revised.

of the BTs and its vertex at the projected intersection of these axes. The heights of the chambers and the SEI optics tables are adjusted so as to be locally level but at the proper position relative to the projected BT axes at their centers.

The optical ray tracing is done in a shifted coordinate system in which the center of the splitting surface of the unfolded interferometer BS is defined as the origin. Positions of the optical components are then transformed (shifted) to the LIGO global coordinate system, unless otherwise noted. The positions and orientations of the optics at each observatory are then determined by transforming¹ into the local horizontal coordinate systems in each building.

7 SOLUTION METHODS

Two methods were used to independently confirm the wedge angles for the COC:

- vector analysis of the reflection and refraction (sequential ray tracing), and
- (non-sequential) optical ray tracing using Optica², including multiple internal reflections.

The wedge angles were calculated with the vector analysis as solutions to nonlinear, constraint equations and then confirmed with Optica. The vector analysis is described in Appendix 2.

8 SOLUTION

8.1. Possible Wedge Orientations

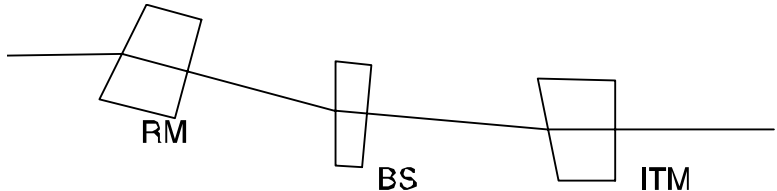
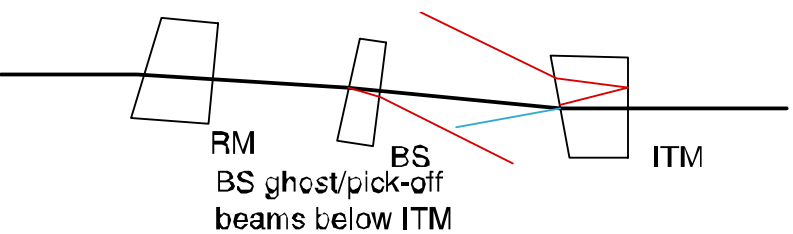
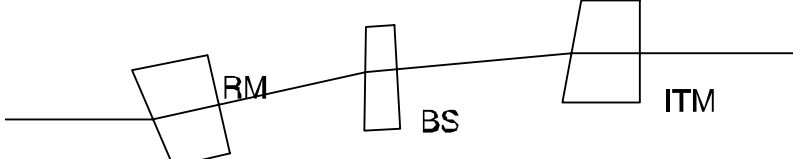
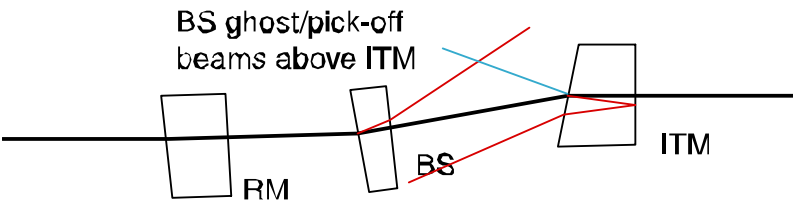
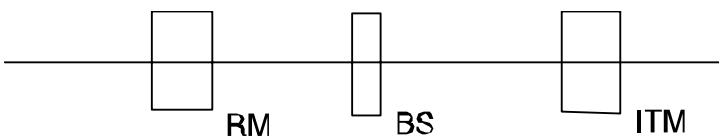
There are five different combinations of wedge angle directions that have been considered to date for the recycling cavities, as indicated in the following table. The need to put the beam line as low as possible in the HAM chambers to fit the triple pendulums (-157 mm in the LIGO global coordinate system) and the need to keep the beam line in the beam tube no closer than 200 mm to the edge of the beam tube baffles, means that we have $\sim\pm 118$ mm for beam path elevation changes through the recycling cavities. If the ITMs and the BS have the same orientation for their vertical wedges (Cases 1 and 3 in the table below), then the total height variation through the recycling cavities exceeds 118 mm for wedge angles which separate the ghost beams (for pick-off beams or beam dumps). In addition, these two cases result in RMs with a greater wedge angle, and high reflectance (HR) surface angle relative to local horizontal, than the two vertical wedge cases for which the ITM and BS wedge angles are not additive in their effect. It is best to minimize the RM angle with respect to the local horizontal in order to minimize vertical to horizontal (length) coupling noise, which is larger for the RM than for the BS and ITMs. (see appendix 1 for details).

For the vertical wedge case with thick side up ITMs and a thick side down BS, (case 2 in the table), the BS pick-off beam is lower than the ITMs. This means that the pick-off mirror must extend below the quadruple pendulum in the ITM chambers; Though possible, it is an awkward arrangement to provide such a long pick-off mirror structure, or pendulum, and not block the main beam.

1. Ibid

2. D. Barnhart, "Optica: A New Generation System for Optical Design and Analysis", version 1.1.0 with a patch for Mathematica 3.0, Wolfram Research, Jan. 95.

Table 2. Summary of RC Optical Wedge Layout Scenarios

#	Case	<i>Refracted Path Schematic, elevation view (BS rotated into the plane and angles exaggerated for clarity)</i>
1	Vertical Wedges: ITM & BS with thick sides up (like LIGO-1)	
2	Vertical Wedges: ITM with thick side up, BS with thick side down	 <p>BS ghost/pick-off beams below ITM</p>
3	Vertical Wedges: ITM and BS with thick sides down	
4	Vertical Wedges: ITM with thick side down, BS with thick side up (current baseline for advanced LIGO)	 <p>BS ghost/pick-off beams above ITM</p>
5	Horizontal Wedges (left/right orientation will mat- ter due to handedness associated with the folded and non-folded interferometers)	

The remaining vertical wedge case, with thick side down ITMs and a thick side up BS, (case 4 in the table), has the BS pick-off beam above the ITMs, which is much easier to accommodate. This case will also permit the maximum lateral separation of the folded and non-folded interferometer beams which may be necessary to permit clearance of the non-folded interferometer beam past the FMy suspension structure of the folded interferometer.

There does not appear to be sufficient space to catch all of the PO beams for an arrangement with horizontal wedges. However, this arrangement is still a possibility if a single RC pick-off beam is

deemed adequate, non-wedged ITM optics are acceptable and the BS wedge angle can be increased. (This is a possible design change under consideration, as mentioned in section 5.)

All of the wedge layout options suffer from a need for a greater BS wedge angle than the currently defined manufacturing limit for initial LIGO; This requires further review. Although subject to further review and investigation, the chosen baseline is case 4. Details for this layout option are given in the next section.

8.2. Baseline Layout

The vertical positions of the beam in the HAM and BSC chambers are depicted in Figure 4. In the LIGO global coordinate system the beam heights are as follows (and as indicated in Table 5):

- HAM Chamber beam height = -157 mm
- ITMx beam height = -80 mm
- ITMy beam height = -88 mm
- BS splitting surface center height = -150

These heights are approximately consistent with a HAM table height of -315 mm (see layout constraint #4 for assumptions) and a BSC table height of 1696 (assuming a quadruple pendulum height¹, from optic center to optic table attachment, of 1776 mm)

A plan view of the recycling cavity layout (with notional folded interferometer positions currently) is shown in the following Figure 5. The planform dimensions used in the sketch in Figure 5 for the suspensions (both the triple and the quad) are as follows 330 mm x 420 mm for the quadruple pendulum. These dimensions allow little clearance for the structure and perhaps insufficient length for the blade flexures of the upper pendulum stages; This requires further review. The separation between the primary and reaction chains of the prototype quadruple pendulum, shown in the elevation view (Figure 4) is much larger than assumed in the planform view (Figure 4). Note that the safety cage structure, which would surround the quadruple pendulum chains in the BSC chambers, is not shown in the elevation view.

1. The quadruple pendulum height is taken from the GEO group's document: "LIGO II Suspension Reference Designs", LIGO-T000012-00, for the mass center to mass center pendulum lengths, plus 30 mm for the top structure which interfaces to the table based on the prototype quadruple pendulum drawing from the GEO, Glasgow group.

Figure (4) Nominal Beam and Optics Table Elevation in the Recycling Cavity: X-Arm

The depicted prototype quad (with ersatz optics) is slightly shorter than the quad length defined in the SUS reference design document.

The triple is from the SUS reference design document, scaled up for the current PRM & SRM diameter of 265 mm.

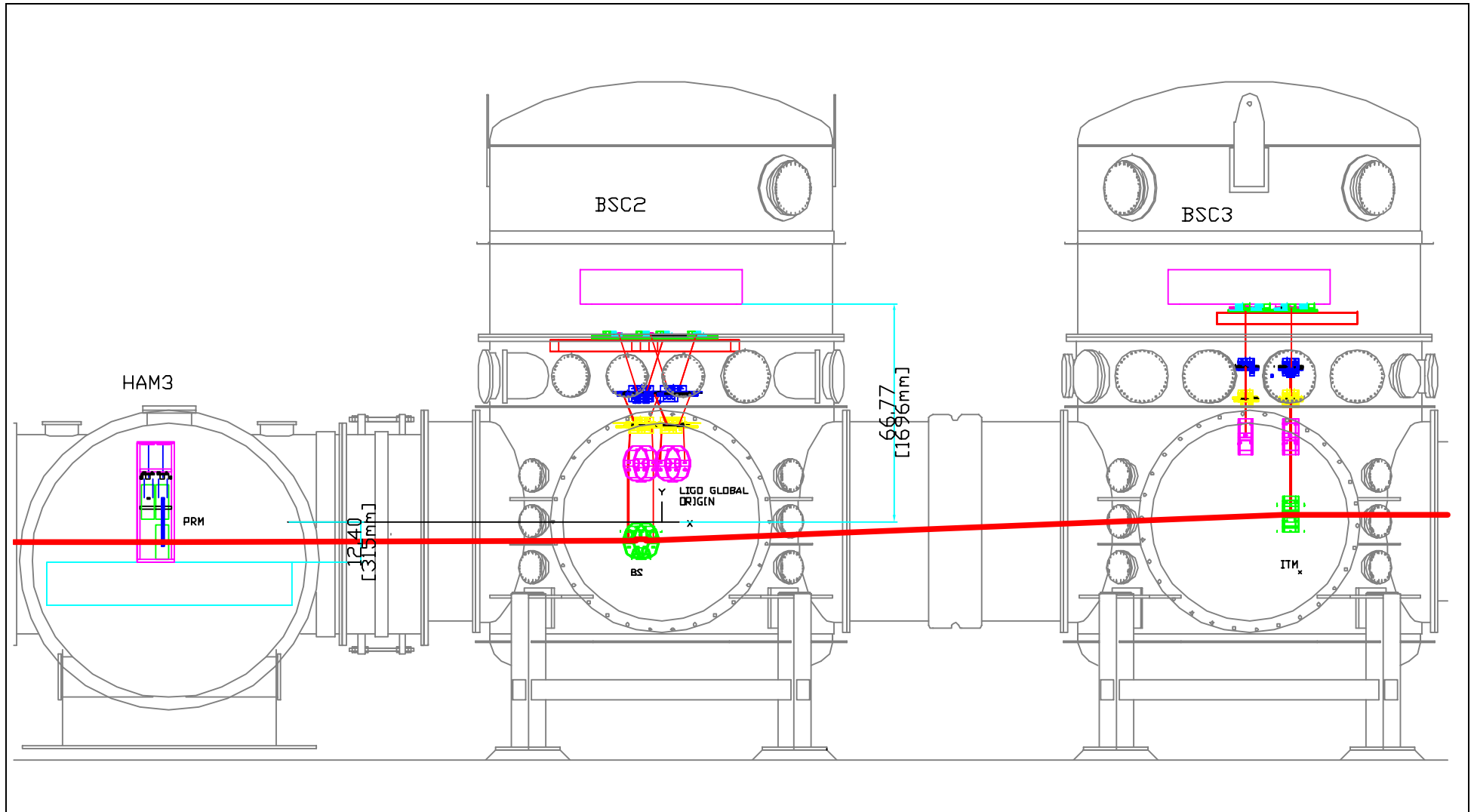
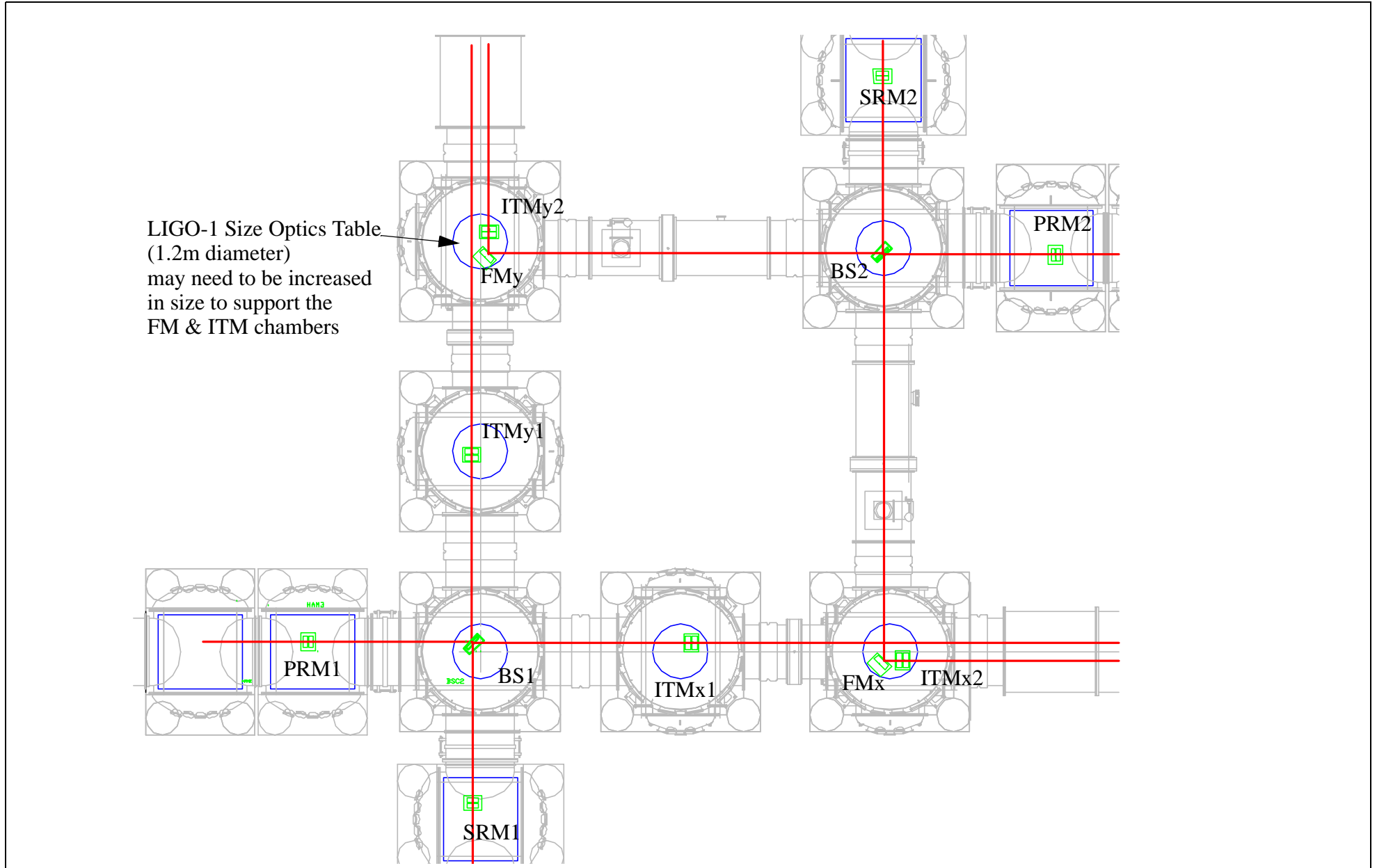


Figure (5) Recycling Cavity Layout

N.B.: (1) The folded interferometer layout is notional; a ray trace analysis is pending.
 (2) The planform dimensions for the suspensions are approximate and not generous.



The wedge angles for the COC for the baseline layout are given in Table 3.

Table 3: RC Core Optics Wedge Angles

(The End Test Mass (ETM) is listed for completeness, but is not part of this RC analysis.)

Interferometer	Optic	Wedge	
		Angle (deg)	Orientation of thick side
Non-Folded Interferometer (#1)	PRM ₁	0.2308 symmetric	up
	SRM ₁	-0.2321 symmetric	down
	BS ₁	1.3000 symmetric	up
	ITM ₁	1.1000 symmetric	down
	ETM ₁	0.5000 single sided	up
Folded Interferometer (#2)	PRM ₂	TBD symmetric	TBD
	SRM ₂	TBD symmetric	TBD
	BS ₂	TBD symmetric	TBD
	FM ₂	0.5000 single sided	up
	ITM ₂	TBD symmetric	TBD
	ETM ₂	0.5000 single sided	up

A comparison to requirements (Table 4) indicates that the baseline layout may be acceptable.

Table 4: Layout Parameter Comparison with Requirements

Criteria#	Parameter	IFO#1	IFO #2	Requirement
1	Lateral separation between IFO beams	TBD		>400 mm
2a	Maximum BS wedge angle	1.3° ^a	TBD	1° 0' max
2b	Maximum ITM wedge angle	1.1°	TBD	3° 0' max
2c	Maximum PRM wedge angle	0.23	TBD	3° 0' max
2d	Maximum SRM wedge angle	0.23	TBD	3° 0' max
3	Wedge angle tolerance	TBD	TBD	± 1'
4	Beam height in HAM chambers ^b	-157 mm	TBD	-157 mm
5a	BS Pickoff Beam Separation from ITM _x (margin after - 2R _{100ppm})	16 mm ^a	TBD	> 30 mm
5b	ITM _x Pickoff Beam Separation from BS (margin after - 2R _{100ppm})	65 mm	TBD	> 30 mm
5c	ITM _y Pickoff Beam Separation from BS (margin after - 2R _{100ppm})	31 mm	TBD	> 30 mm
6a	BS 1st ghost separation at the ITMs (margin after - 2R _{100ppm})	< 0, ITM _y ^a	TBD	> 30 mm
6b	ITM _x 1st ghost separation at the BS (margin after - 2R _{100ppm})	75 mm	TBD	> 30 mm
6c	ITM _y 1st ghost separation at the BS (margin after - 2R _{100ppm})	41 mm	TBD	> 30 mm
6d	RM 1st ghost separation at the BS (margin after - 2R _{100ppm})	< 0 ^c	TBD	> 30 mm
7	Beam line to baffle edge separation in the beam tube (backscatter limit)	281	TBD	> 200 mm
8	Length sensing noise due to optic wedge & pitch angle coupling (as a fraction of a FP surface contribution)	0.50, seismic 0.17, thermal	TBD	< 1, seismic < 0.28, thermal
9 to 13	constraints	all are met	TBD	see section 4

- a. Need to revisit the BS maximum wedge angle criteria. BS pick-off separation would be increased with a larger BS wedge angle.
- b. in the LIGO global coordinate system
- c. Requires beam dumps on the BS suspension structure and a beam dump to catch the RM ghost beam reflection off of the BS, as in LIGO-1.

The specific locations and orientations of the RC COC are given in Table 5.

Table 5: RC Core Optics Position & Orientation

a) $\{\hat{i}, \hat{j}, \hat{k}\}$ are the coordinate system vector triad associated with the coordinate directions (x,y,z).

(b) The notation for points and unit normal vectors is per Figures 11 and 12 of Appendix 2.

IFO	Optic	Surface ^a	Center Coordinate				Surface Orientation (unit normal vector; direction cosines)				
			pt.	X (mm)	Y (mm)	Z (mm)	\hat{n}	\hat{i}	\hat{j}	\hat{k}	
#1	PRM1	AR	p2	-3930.48	222.355	-156.562	n2	-0.999983	0.0000951835	-0.00583974	
	PRM1	HR	p3	-3830.99	222.346	-156.382	n3	-0.999998	0.0000951849	-0.00181133	
	BS1	BS	p4	-200	222	-149.805	n4	-0.707081	0.707075	0.00896563	
	BS1	AR-x	p5	-129.492	202.038	-149.967	n5	-0.706755	0.70675	0.0316497	
	BS1	AR-aps	p5p	-180.042	151.497	-150.791	n5	-0.706755	0.70675	0.0316497	
	ITMx	AR	p6	4663.39	202.038	-80.5053	n6	-0.999816	-1.1284×10^{-20}	0.0191974	
	ITMx	HR	p7	4784.13	202.038	-80.5053	n7	-1	0	0	
	ITMy	AR	p8	-200.	4508.71	-87.6796	n8	0.	-0.999816	0.0191974	
	ITMy	HR	p9	-200.	4629.44	-87.6796	n9	0	-1	0	
	SRM1	AR	p10	-179.69	-3257.04	-157.	n10	-0.000103337	0.999998	0.00182167	
	SRM1	HR	p11	-179.68	-3357.55	-157.183	n11	-0.000103336	0.999983	0.0058731	
		ETM _{x1}	HR	p12	4000161	200	-202	\hat{n}_{12}	-1	0	0
		ETM _{y1}	HR	p14	-200	3999834	-198	\hat{n}_{14}	0	-1	0

Table 5: RC Core Optics Position & Orientation

- a) $\{\hat{i}, \hat{j}, \hat{k}\}$ are the coordinate system vector triad associated with the coordinate directions (x,y,z).
 (b) The notation for points and unit normal vectors is per Figures 11 and 12 of Appendix 2.

IFO	Optic	Surface ^a	Center Coordinate				Surface Orientation (unit normal vector; direction cosines)			
			pt.	X (mm)	Y (mm)	Z (mm)	\hat{n}	\hat{i}	\hat{j}	\hat{k}
#2	PRM ₂	HR	p ₃	TBD	TBD	TBD	\hat{n}_3	TBD	TBD	TBD
	SRM ₂	HR	p ₃	TBD	TBD	TBD	\hat{n}_3	TBD	TBD	TBD
	BS ₂	BS	p ₄	TBD	TBD	TBD	\hat{n}_4	TBD	TBD	TBD
	FM _x	HR	p ₉	TBD	TBD	TBD	\hat{n}_9	TBD	TBD	TBD
	ITM _{x2}	HR	p ₁₀	TBD	TBD	TBD	\hat{n}_{10}	TBD	TBD	TBD
	FM _y	HR	p ₆	TBD	TBD	TBD	\hat{n}_6	TBD	TBD	TBD
	ITM _{y2}	HR	p ₇	TBD	TBD	TBD	\hat{n}_7	TBD	TBD	TBD
	ETM _{x1}	HR	p ₆	TBD	TBD	TBD	\hat{n}_6	TBD	TBD	TBD
	ETM _{y1}	HR	p ₈	TBD	TBD	TBD	\hat{n}_8	TBD	TBD	TBD

a. HR = High Reflectance, BS = beamsplitting, AR = Anti-Reflectance

The unit length ray vectors (using the notation of Appendix 2) are given in Table 6.

Table 6: RC Core Optics Ray Parameters

IFO	Description	Ray	Ray unit vector (direction cosines)		
			\hat{i}	\hat{j}	\hat{k}
#1	PRM1 AR input	u2	1.	-0.0000951851	-2.5693×10^{-14}
	PRM1 HR input	u3	0.999998	-0.0000951849	0.00181133
	BS bs input	u4	0.999998	-0.0000951849	0.00181133
	BS ar input	u5	0.962178	-0.272412	-0.00220381
	BS arp input	w4p	0.272349	-0.962105	-0.0134497
	ITMx AR input	u6	0.999895	-8.51766×10^{-21}	0.0144911
	ITMx HR input	u7	1	0	0
	ITMy AR input	u8	0.	0.999895	0.0144911
	IMTy HR input	u9	0	1	0
	SRM1 HR input	u10	0.000103337	-0.999998	-0.00182167
	SRM1 AR input	u11	0.000103337	-0.999998	-0.00182167
	ETM _x input ray	\hat{u}_6	1	0	0
	ETM _y input ray	\hat{u}_8	0	1	0

Table 6: RC Core Optics Ray Parameters

IFO	Description	Ray	Ray unit vector (direction cosines)		
			\hat{i}	\hat{j}	\hat{k}
#2	PRM input ray		TBD	TBD	TBD
	SRM input ray		TBD	TBD	TBD
	BS input ray		TBD	TBD	TBD
	FM _x input ray		TBD	TBD	TBD
	ITM _x input ray		TBD	TBD	TBD
	FM _y input ray		TBD	TBD	TBD
	ITM _y input ray		TBD	TBD	TBD
	ETM _x input ray	\hat{u}_6	1	0	0
	ETM _y input ray	\hat{u}_8	0	1	0

The physical path length (not optical path length), folded into a common plane, versus elevation is given in Figures 5 and 6, for the non-folded (#1) and folded (#2) interferometers respectively.

Figure (6) IFO #1 Pathlength vs. Height

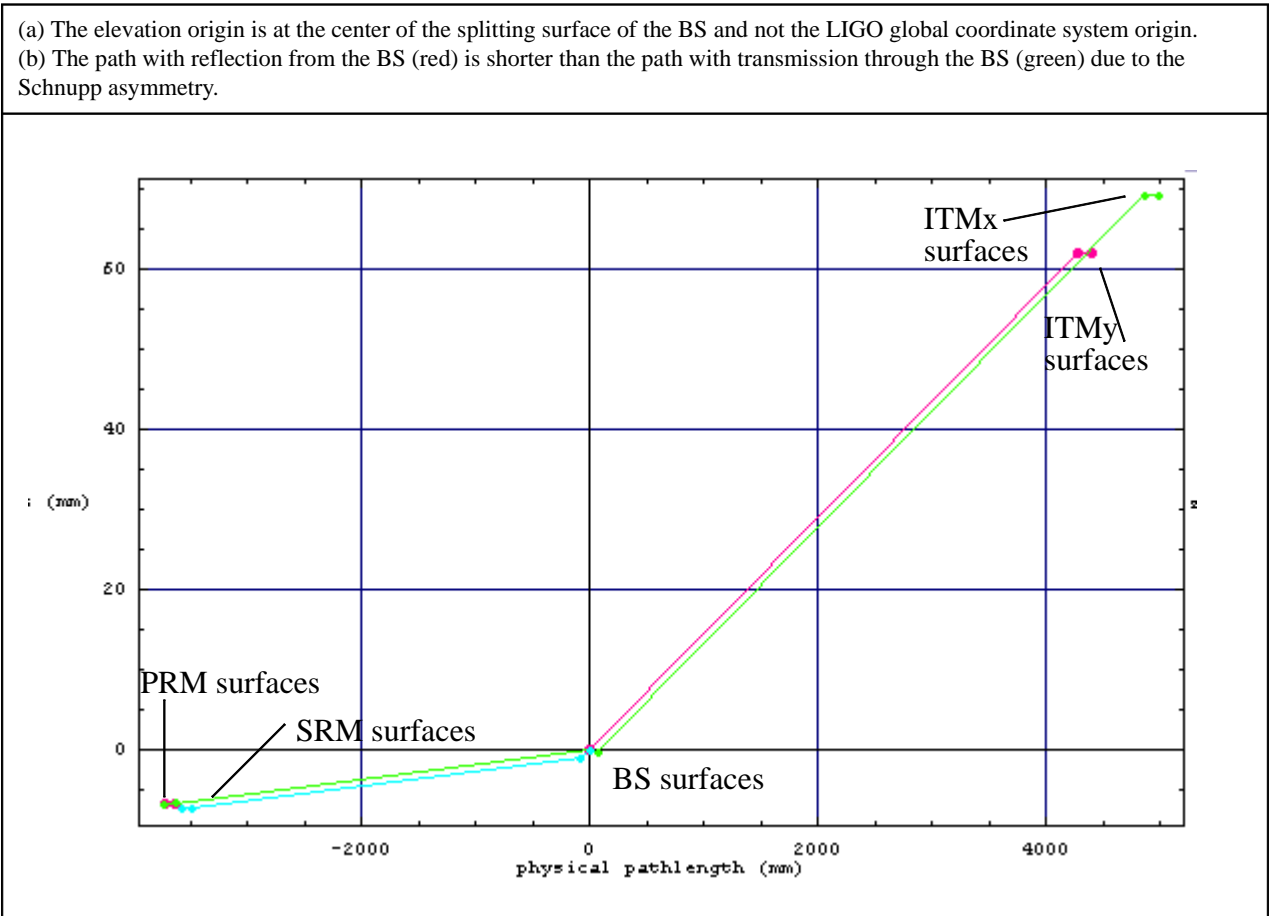
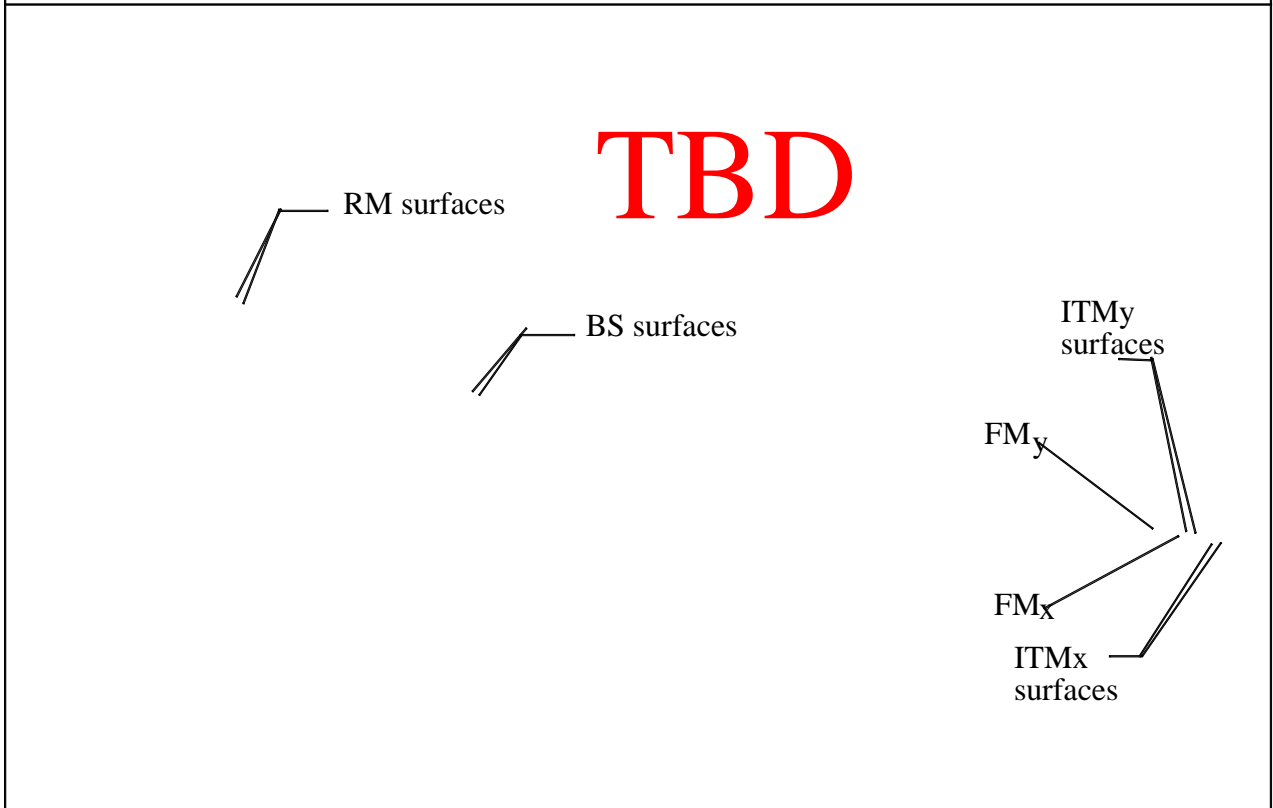


Figure (7) IFO #2 Pathlength vs. Height

(a) The elevation origin is at the center of the splitting surface of the BS and not the LIGO global coordinate system origin.
(b) The path with reflection from the BS (red) is longer than the path with transmission through the BS (green) due to the Schnupp asymmetry.



The IFO #1 RC optical layout in Optica is given in Figure 8. **Note: The Figure 8 plots are for case 2 of table 2, not the baseline: case 4 of table 2; These figures will be revised.**

Figure (8) Optica IFO #1 RC Layout (isometric view)

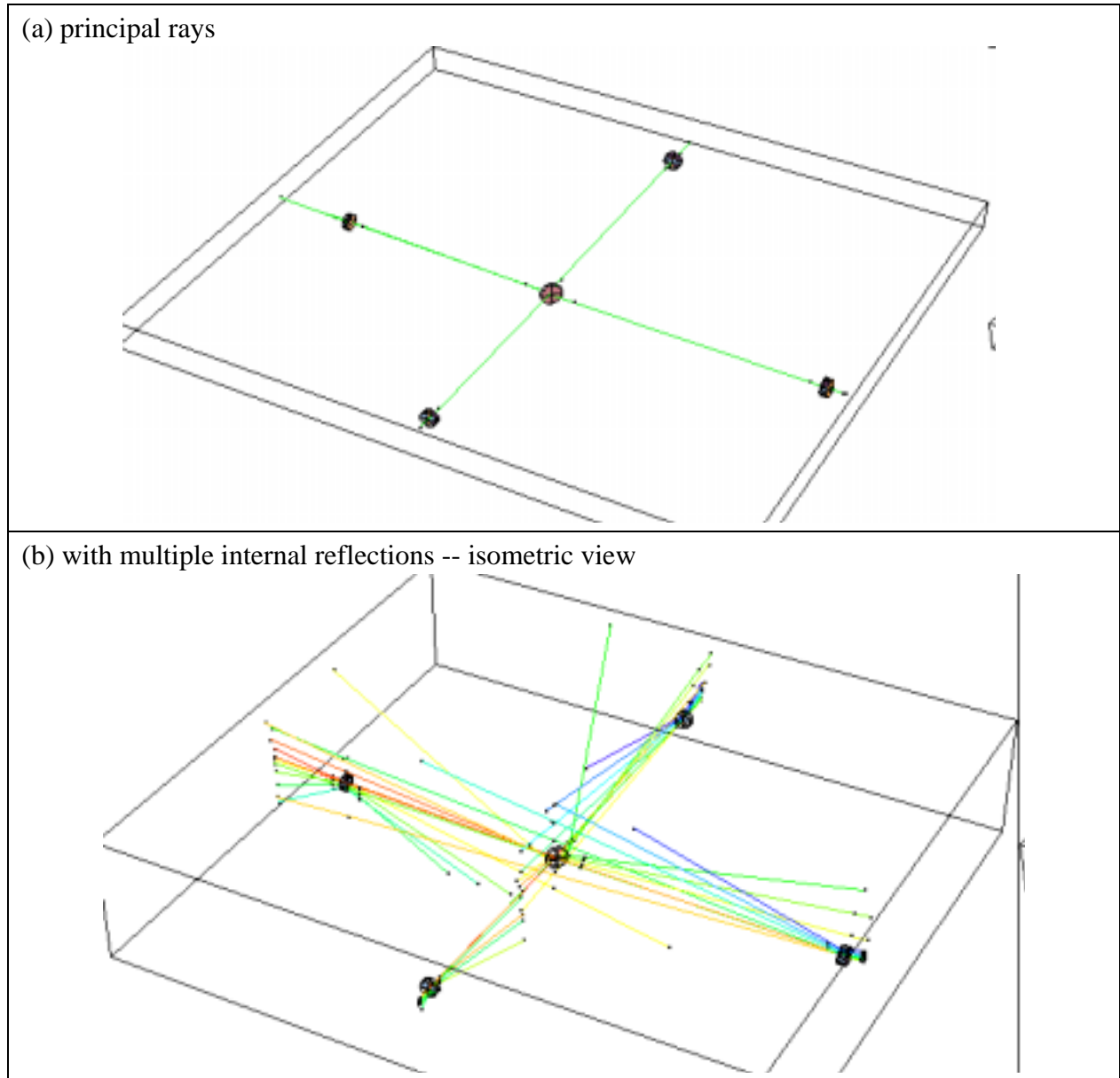
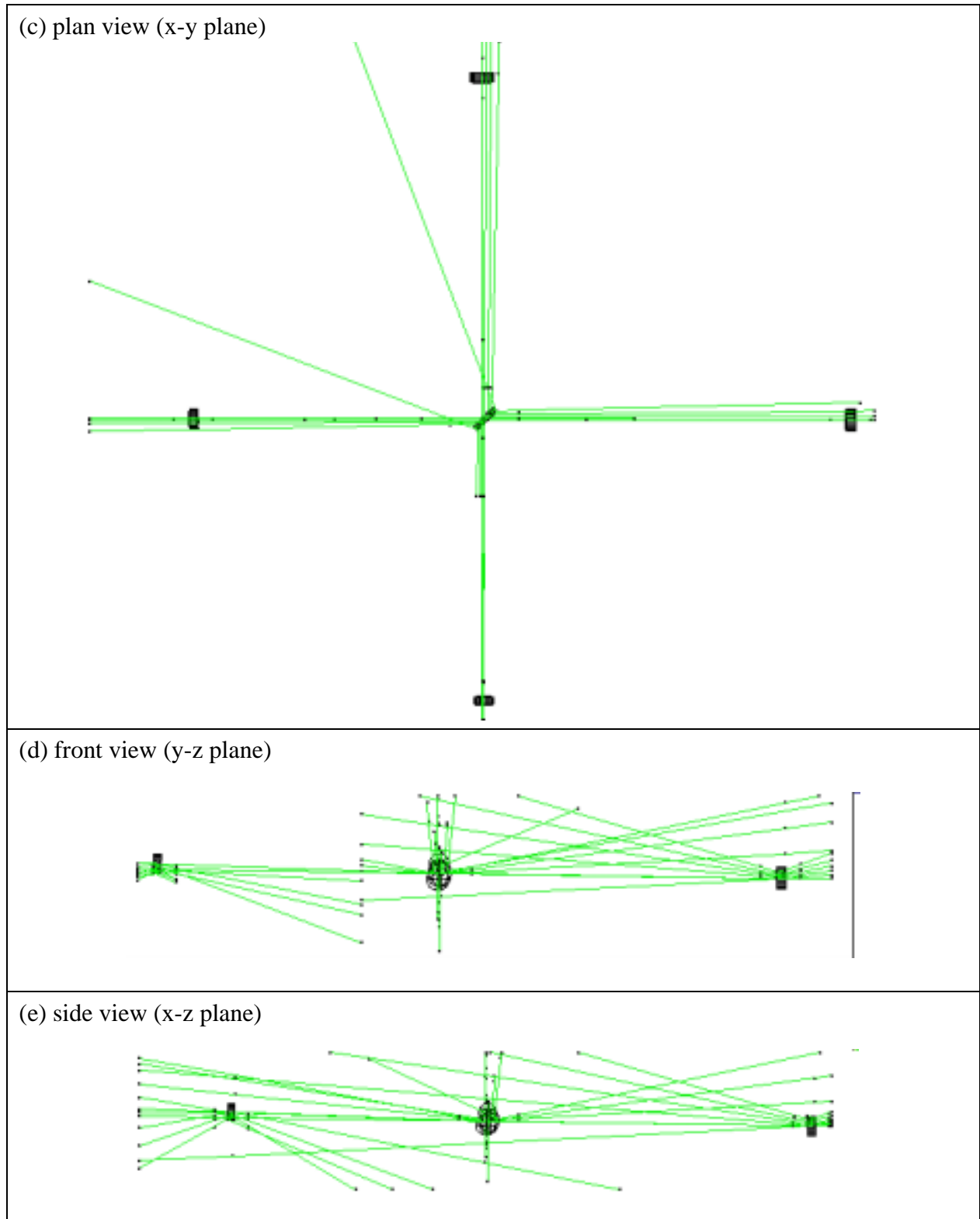


Figure (8) Optica IFO #1 RC Layout (isometric view)



The IFO #2 RC optical layout in Optica is given in Figure 8.

Figure (9) Optica IFO #2 RC Layout (isometric view)

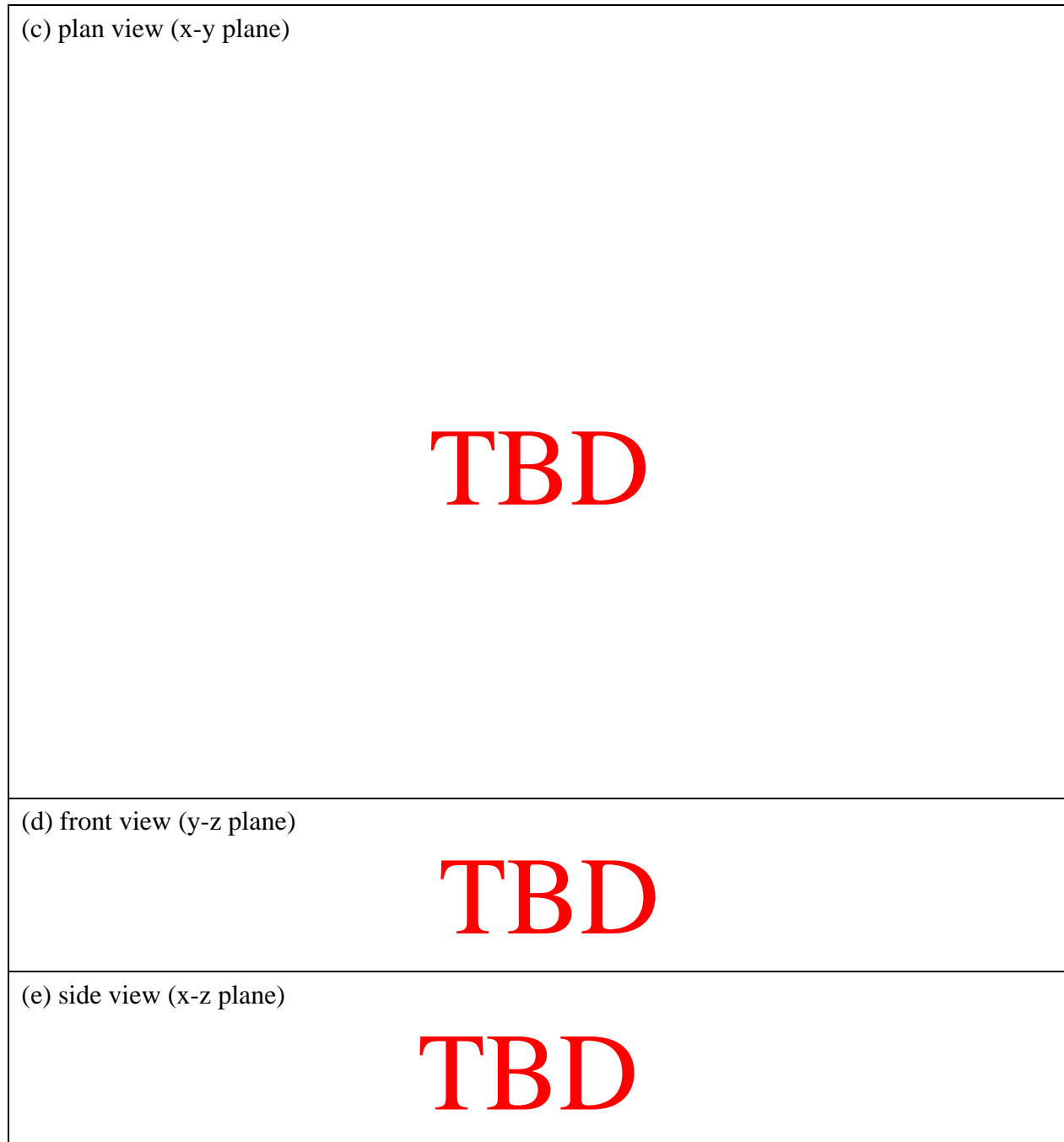
(a) principal rays

TBD

(b) with multiple internal reflections -- isometric view

TBD

Figure (9) Optica IFO #2 RC Layout (isometric view)



APPENDIX 1 VERTICAL DISPLACEMENT NOISE COUPLING

Vertical motion of the PRC & SRC optics will couple into length noise if the surfaces are not vertical¹. The seismic noise and thermal noise contributions due to coupling from vertical ITM motion to length change due to the earth's curvature (resulting in 0.6 mrad max. ITM HR surface angle relative to vertical) is significant. The wedge angles, which are required to separate ghost beams and provide angular alignment sensing beams (pickoff beams), also cause the surfaces not to be vertical. The basic problem is to separate the ITM pickoff beam (and 1st ghost beam) at the BS by about 1 optic diameter:

$$\theta \approx \frac{\text{atan}\left(\frac{d}{l}\right)}{2} = \frac{\text{atan}\left(\frac{0.265}{3.6}\right)}{2} = 37\text{mrad} \quad (1)$$

This ray deviation angle is large and suggests that there may be significant coupling from vertical motion to length signal (compare to 0.62 mrad in the Fabry-Perot cavities).

In transmission, vertical motion of a wedged optic causes a phase change due to an optical path difference (OPD). On the RC side, vertical motion of the ITM and the BS couple to the length sensing noise as follows:

$$\Phi_{(ITM,opd)} = \left(\frac{2\pi}{\lambda}\right)(n-1)\alpha_{ITM}z \quad (2)$$

$$\Phi_{(BS,opd)} = \left(\frac{2\pi}{\lambda}\right)(n-1)\alpha_{BS}z \quad (3)$$

where

n = index of refraction = 1.44963² for fused silica, or = 1.7546 for sapphire³

α_i = wedge angle of optic i

z = vertical motion (thermal or seismic)

Vertical motion of the reflective surfaces in the RC couple to the length sensing noise as follows:

$$\Phi_{BS} = \left(\frac{2\pi}{\lambda}\right)2\beta_{BS}z \quad (4)$$

-
1. Adapted from the original formulation for initial LIGO due to D. Shoemaker, G. Gonzalez and D. Coyne.
 2. Optica, index of refraction for fused silica at 1.064 microns
 3. Handbook of Infrared Optical Materials, Klocke, P.(ed), Marcel Dekker, 1991, index of refraction for sapphire at 1.064 microns

$$\Phi_{FM} = \left(\frac{2\pi}{\lambda}\right) 2\beta_{FM}z \quad (5)$$

$$\Phi_{PRM} = \left(\frac{2\pi}{\lambda}\right) \left(\frac{2\beta_{PRM}}{CM}\right)z \quad (6)$$

$$\Phi_{SRM} = \left(\frac{2\pi}{\lambda}\right) \left(\frac{2\beta_{SRM}}{CM}\right)z \quad (7)$$

where

β = angle from local vertical of the reflective surface of optic i

CM = common mode rejection factor = ~30

where the factor of 2 is due to mirror reflection. The motion of the recycling mirror itself is less bothersome for the GW output by the common mode rejection (CM) of the interferometer. The CM rejection is of the order of ~30 to ~100 (set CM = 30 to be conservative).

Motion of a HR ITM surface in the FP cavity contributes to the noise floor as follows:

$$\Phi_{fpi} = \left(\frac{2\pi}{\lambda}\right) \beta_i G_{fp} z \quad (8)$$

where

G_{fp} = 800 = Fabry-Perot effective bounce factor, or phase change amplification

β_i = angle from local vertical of the reflective surface of ITM i

In general, the motion of the surfaces in the measurement band can be taken to be uncorrelated, so that the net contribution is the RSS of the individual contributions; the exceptions are the FMs in the folded interferometer since they share an optics table with their corresponding ITM. However, the FMs point in a different direction, so are at most $\sqrt{2}$ correlated, and they are probably not well correlated along their common axis. So as a simplification, we'll take all to be uncorrelated. The net noise contribution for the folded IFO is then approximately:

$$\Phi_{total}^2 = \Phi_{PRM}^2 + \Phi_{SRM}^2 + \Phi_{BS}^2 + 2\Phi_{FM}^2 + \Phi_{fp}^2 + 2\Phi_{(ITM, opd)}^2 + \Phi_{(BS, opd)}^2 \quad (9)$$

where, the contribution from the Fabry-Perot cavity is:

$$\Phi_{fp}^2 = \Phi_{ITMx}^2 + \Phi_{ITMy}^2 + \Phi_{ETMx}^2 + \Phi_{ETMy}^2 \quad (10)$$

The surface normal vector angle with the local horizontal is dependent upon the site as indicated

in the following table. Each of the surface normal vectors should be transformed (rotated) into the local horizontal coordinate system of each LIGO building; Since this is a small correction for the RC optics, this is only done for the Fabry-Perot optics in this analysis.

Table 7. Fabry-Perot angles with respect to the local horizontal (mrad)

<i>Station - Direction</i>	<i>LIGO Hanford Observatory</i>	<i>LIGO Livingston Observatory</i>
Vertex - X	0.619	0.312
Vertex - Y	0.012	0.611
X-End - X	0.008	0.314
Y-End - Y	0.639	0.019

The same expressions apply to the non-folded IFO with the exception that there are no FMs in the non-folded IFO. Rearranging this equation:

$$\xi = \left(\frac{\Phi_{total}^2}{\Phi_{fp}^2} - 1 \right)^{1/2} = \left(\frac{\Phi_{PRM}^2 + \Phi_{SRM}^2 + \Phi_{BS}^2 + 2\Phi_{FM}^2 + 2\Phi_{(ITM, opd)}^2 + \Phi_{(BS, opd)}^2}{\Phi_{fp}^2} \right)^{1/2} \quad (11)$$

The wedge and surface angles relative to vertical for the folded and non-folded IFOs are given in Table 7

Table 8. Optic Surface Angular Deviations (mrad) from Vertical

N.B.: Angles are in the global coordinate system, not the local vertical coordinate systems.

Optic (surface)		IFO #1	IFO #2
PRM(hr)	β	1.8	TBD
SRM(hr)	β	1.8	TBD
BS(bs)	β	9.0	TBD
	α	22.7	TBD
FMx(hr)	β	NA	TBD
ITMx(ar)	α	19.2	TBD
FMy(hr)	β	NA	TBD
ITMy(ar)	α	19.2	TBD

Seismic Displacement Noise Coupling

Seismic noise does not dominate in the gravitational detection wave band¹. Nonetheless, we want to limit the contribution of seismic noise coupling from non-vertical RC optics so that the motion at 10 Hz and below is not significantly enhanced. Limiting the contribution from the RC optics to be no more than from the test masses seems appropriate, i.e.

$$\xi_{seismic} \leq 1 \quad (12)$$

From the Advanced LIGO System Design document, the following vertical displacement noise limits are derived, based on the required horizontal displacement noise spectrum limit at 10 Hz and the vertical to horizontal coupling factors, under the assumption that vertical noise coupling dominates:

$$z_{TM} = 1 \times 10^{-19} / 0.001 = 1 \times 10^{-16} \text{ m} / \sqrt{\text{Hz}}$$

$$z_{RM} = 3 \times 10^{-16} / 0.006 = 5 \times 10^{-14} \text{ m} / \sqrt{\text{Hz}}$$

$$z_{BS} = 2 \times 10^{-17} / 0.014 = 1.4 \times 10^{-15} \text{ m} / \sqrt{\text{Hz}}$$

Consequently, for seismic noise coupling at 10 Hz,

$$\xi_{\text{non-folded, seismic}} = 0.50 \text{ for LLO, } 0.43 \text{ for LHO} \quad (13)$$

$$\xi_{\text{folded, seismic}} = \text{TBD} \quad (14)$$

Thermal Displacement Noise Coupling

For thermal noise coupling, which can limit the interferometer sensitivity (at low laser power), we take as a criteria that each RC surface should contribute no more than 1/10 of the contribution of the FP surfaces, i.e.

$$\xi \leq \frac{\sqrt{8}}{10} = 0.28 \quad (15)$$

The following thermal noise estimates, at 10Hz, are from the Suspension Reference Design document:

$$x_{TM} = 9 \times 10^{-20} \text{ m} / \sqrt{\text{Hz}}$$

$$x_{RM} = 9 \times 10^{-19} \text{ m} / \sqrt{\text{Hz}}$$

for the horizontal displacement noise of the test masses and recycling mirrors, respectively. Assuming that the vertical component of the thermal noise is proportional to the horizontal component, and assuming (for lack of an estimate) that the BS suspension thermal noise is a factor of 2 lower than the RM suspension thermal noise (and an factor of 5 higher than a TM suspension):

$$\xi_{\text{non-folded, thermal}} = 0.17 \text{ for LLO, } 0.15 \text{ for LHO} \quad (16)$$

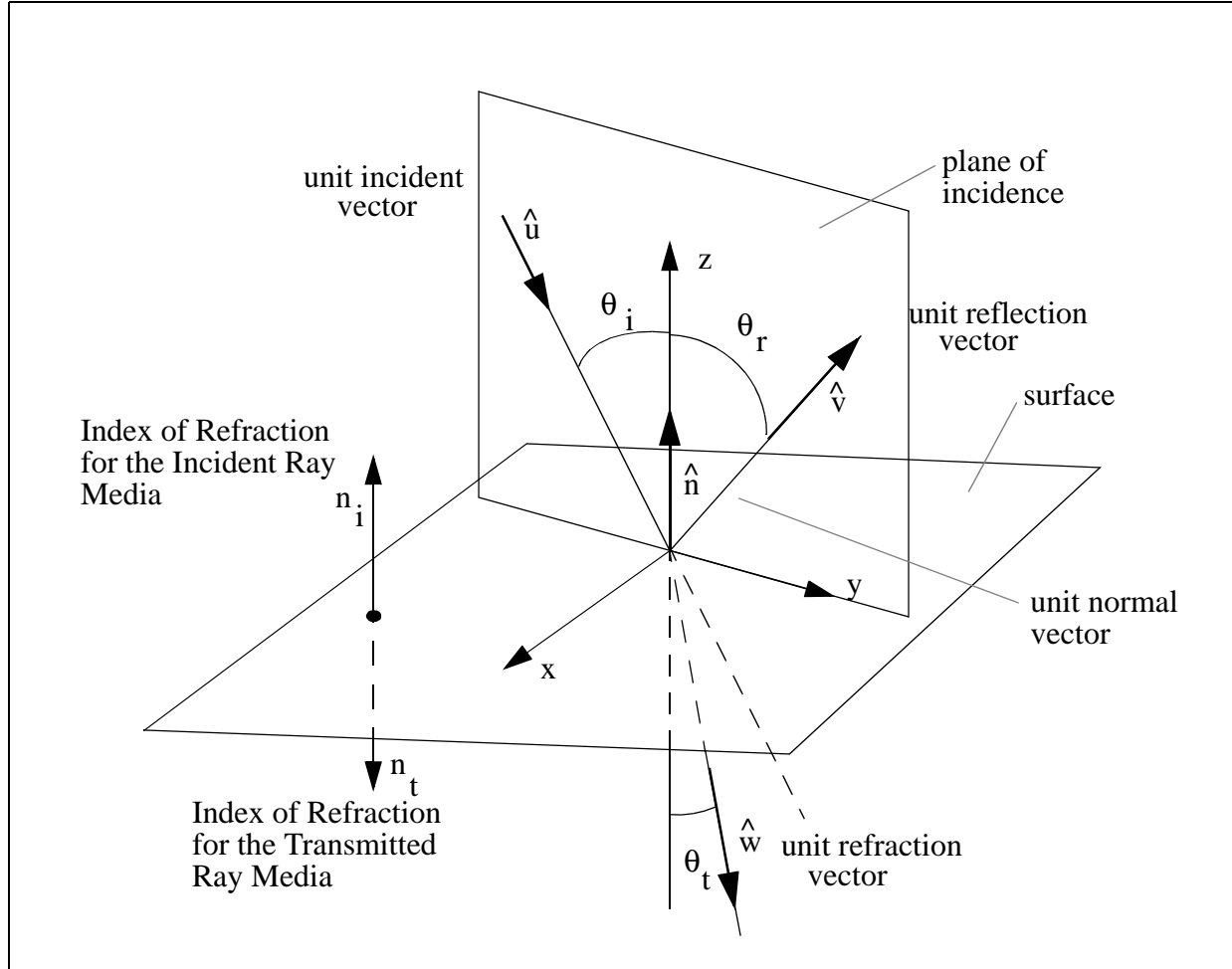
$$\xi_{\text{folded, thermal}} = \text{TBD} \quad (17)$$

1. Suspension thermal and internal thermal noise will dominate if the photon pressure noise is reduced.

APPENDIX 2 VECTOR ANALYSIS

Consider a surface at which the index of refraction changes discretely (Fig. 9) and define a “natu-

Figure (10) Geometry for Refraction and Reflection at a Surface



ral” coordinate system in the plane of incidence with the $+z$ -axis coincident with the outward surface normal vector, \hat{n} , and the y axis at the intersection of the plane of incidence and the surface. Using the notation of Figure 6, and $\{\hat{i}, \hat{j}, \hat{k}\}$ as the coordinate system unit vector triad corresponding to $\{x, y, z\}$:

$$\hat{n} = \hat{k} \quad (18)$$

$$\hat{i} = \frac{\hat{u} \times \hat{n}}{|\hat{u} \times \hat{n}|} \quad (19)$$

$$\hat{j} = \hat{n} \times \hat{i} \quad (20)$$

The law of reflection is:

$$\Theta_i = \Theta_r \quad (21)$$

or,

$$\hat{v} = (\hat{u} \cdot \hat{j})\hat{j} - (\hat{u} \cdot \hat{k})\hat{k} \quad (22)$$

The law of refraction is:

$$n_i \sin \Theta_i = n_t \sin \Theta_t \quad (23)$$

or,

$$n_i(\hat{u} \cdot \hat{j}) = n_t(\hat{w} \cdot \hat{j}) \quad (24)$$

Since,

$$(\hat{w} \cdot \hat{k})^2 + (\hat{w} \cdot \hat{j})^2 = 1 \quad (25)$$

The refraction vector can be expressed as:

$$\hat{w} = \left(\frac{n_i}{n_t}\right)(\hat{u} \cdot \hat{j})\hat{j} - \left\{1 - \left(\frac{n_i}{n_t}\right)^2 (\hat{u} \cdot \hat{j})^2\right\}^{\frac{1}{2}} \hat{k} \quad (26)$$

These equations for reflection and refraction were defined as functions in Mathematica and used to propagate rays (unit vectors), \hat{u}_m , incident upon surface, S_m , into reflected rays, \hat{v}_m , and refracted rays, \hat{w}_m :

$$\hat{v}_m = \text{Reflect}[\hat{u}_m, \hat{n}_m] \quad (27)$$

$$\hat{w}_m = \text{Refract}[\hat{u}_m, \hat{n}_m, n_i, n_t] \quad (28)$$

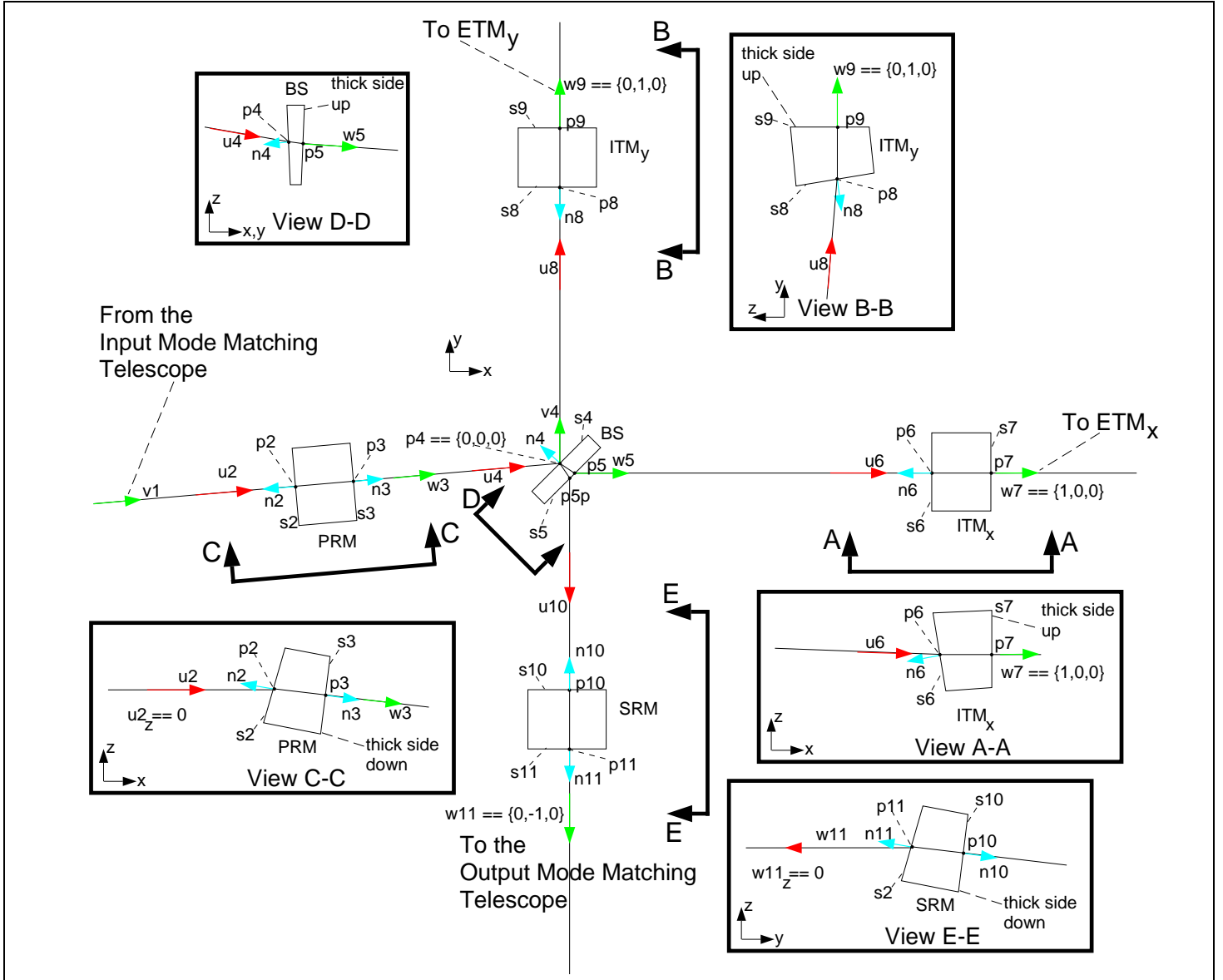
The reflected rays and refracted rays then become the incident rays, \hat{u}_{m+1} , for the next surface, S_{m+1} .

The positions of the ray/surface intercept points are found by simply propagating the rays with the separation distances between the optics, $d_{(m+1)}$:

$$P_{(m+1)} = P_m + d_{m,(m+1)} \hat{u}_{(m+1)} \quad (29)$$

The surfaces of the optics in the non-folded and folded IFOs are numbered as indicated in Figures 11 and 12, respectively. The solution proceeds in stepwise fashion, first for the non-folded and

Figure (11) Ray Vector Notation for the LIGO Recycling Cavity (Non-Folded IFO #1)



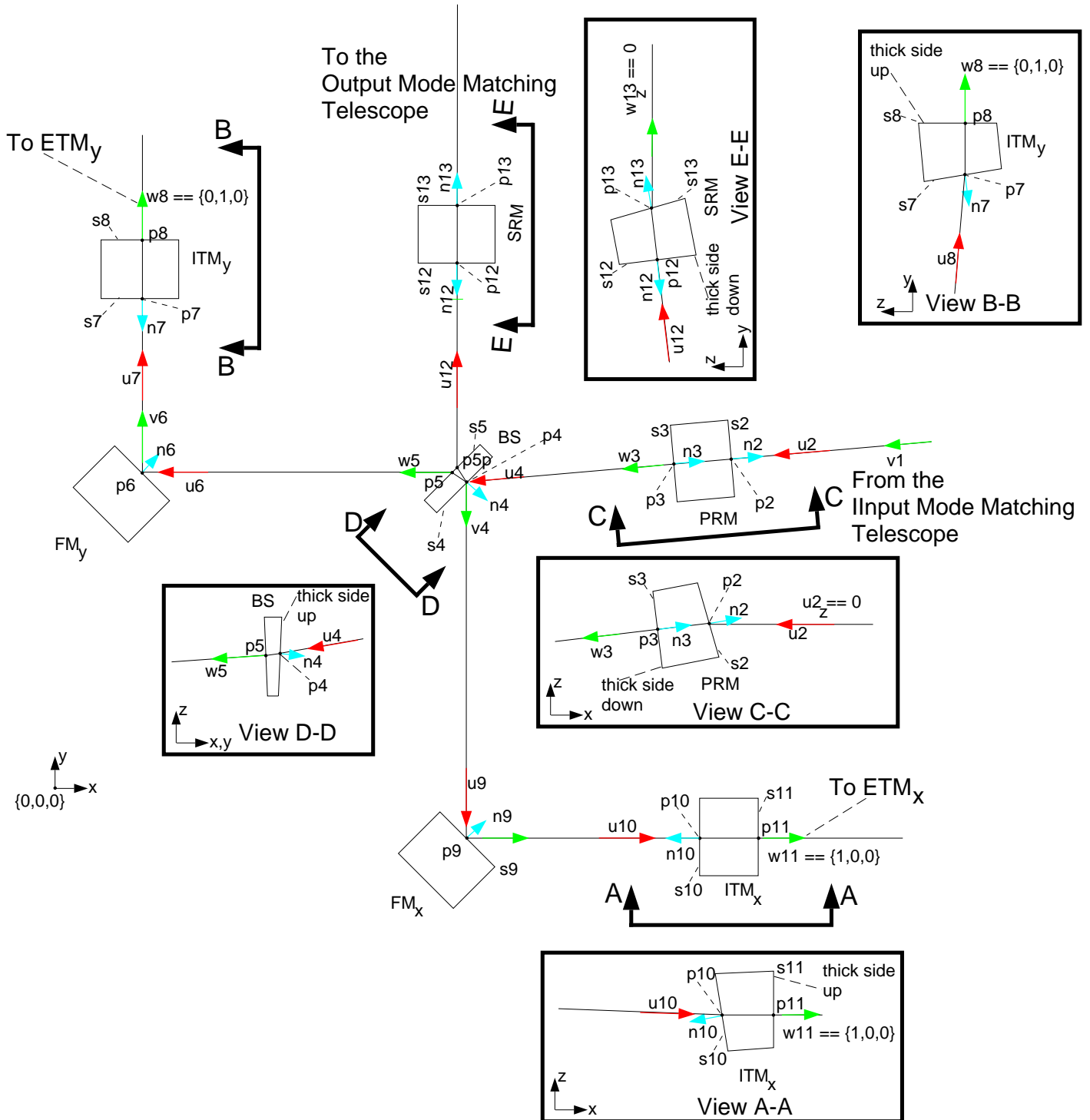
then for the folded IFO:

Step 1) The non-folded IFO Fabry-Perot cavities are aligned along the coordinate axes, so that:

$$w_8 = u_9 = -v_9 = -n_9 = w_9 = \{0,1,0\} \quad (30)$$

$$w_6 = u_7 = -v_7 = -n_7 = w_7 = \{1,0,0\} \quad (31)$$

Figure (12) Ray Vector Notation for the LIGO Recycling Cavity (Folded IFO #2)



for the non-folded IFO (and similarly for the folded IFO).

Step 2) The wedge angles of the ITMx and ITMy optics were selected to give a first reflection off of the AR surface (i.e. vectors v_6 and v_8 for the non-folded IFO and vectors v_7 and v_{10} for the folded IFO) which meet the separation criteria.

$$\hat{n}_8 = R_{\alpha_{8,9}} \hat{n}_9 \quad (32)$$

$$\hat{u}_8 = -\text{Refract}[-\hat{w}_8, -\hat{n}_8, n_{\text{optic}}, n_{\text{vacuum}}] \quad (33)$$

$$\hat{v}_8 = \text{Reflect}[\hat{u}_8, \hat{n}_8] \quad (34)$$

$$\delta_{8,4} = p_4 - (p_8 + d_{4,8} \hat{v}_8) \quad (35)$$

where

$$n_{\text{optic}} = 1.44963 \text{ @ } \lambda = 1.064 \text{ mm for fused silica}^1 \text{ (PRM, SRM, BS)}$$

$$= 1.7546 \text{ @ } \lambda = 1.064 \text{ mm for sapphire}^2 \text{ (ITM, ETM)}$$

$$n_{\text{vacuum}} = 1$$

R_θ = 3D rotation matrix for the angle θ

$\alpha_{m,m+1}$ = wedge angle for the optic with surfaces m and $m+1$

A similar equation applies for the rays associated with ITMx.

Step 3) With the BS output ray directions (\hat{u}_8 in reflection and \hat{u}_6 in transmission) determined, it is possible to calculate the BS orientation, \hat{n}_4 , if a BS wedge angle, α_{45} , is assumed. Simultaneously solve:

$$\hat{u}_8 = \text{Reflect}[\hat{u}_4, \hat{n}_4] \quad (36)$$

$$\hat{u}_6 = \text{Refract}[\text{Refract}[\hat{u}_4, \hat{n}_4, n_{\text{vacuum}}, n_{\text{optic}}], \hat{n}_5, n_{\text{optic}}, n_{\text{vacuum}}] \quad (37)$$

given,

$$\hat{n}_5 = R_{\alpha_{4,5}} \hat{n}_4 \quad (38)$$

1. Optica, index of refraction for fused silica at 1.064 microns

2. Handbook of Infrared Optical Materials, Klocke, P.(ed), Marcel Dekker, 1991, index of refraction for sapphire at 1.064 microns

This is effectively 2 equations in 2 unknowns (the ‘tip’ and ‘tilt’ of the BS, \hat{n}_4). The assumed BS wedge angle, α_{45} , is checked (iterated) to assure that the first ghost beams are well separated from the ITMs. The result of this step is not only the BS orientation normal vector, \hat{n}_4 , but also the input ray normal vector, \hat{u}_4 .

Step 4) With the input ray vector to the BS known, \hat{u}_4 , the stipulation that the PRM HR surface be oriented in this direction (since it forms an input mirror for the PRC) and the requirement that the input to the PRM (i.e. the output of the IO mode matching telescope) be oriented parallel to the x-y global plane, we can determine the PRM wedge angle:

$$\hat{w}_2 = \hat{u}_3 = \hat{w}_3 = \hat{u}_4 \quad (39)$$

$$\hat{n}_3 = -\hat{w}_2 \quad (40)$$

$$\hat{n}_2 = R_{\alpha_{2,3}} \hat{n}_3 \quad (41)$$

$$\hat{u}_2 = -\text{Refract}[-\hat{w}_2, -\hat{n}_2, n_{\text{optic}}, n_{\text{vacuum}}] \quad (42)$$

The PRM wedge angle, α_{23} , is determined by minimizing the z component of the input ray vector to the PRM:

$$\hat{u}_2 \cdot \hat{k} \equiv 0 \quad (43)$$

Step 5) With the BS wedge angle, α_{45} , and orientation, \hat{u}_4 , determined, the anti-symmetric port (APS) ray vector, \hat{w}_{11} , and the SRM wedge angle, $\alpha_{10,11}$, can be found:

$$\hat{v}_4 = \hat{u}_8 \quad (44)$$

$$\hat{w}_{4p} = \text{Refract}[-\hat{v}_4, \hat{n}_4, n_{\text{vacuum}}, n_{\text{optic}}] \quad (45)$$

$$\hat{w}_{5p} = \text{Refract}[\hat{w}_{4p}, \hat{n}_5, n_{\text{optic}}, n_{\text{vacuum}}] \quad (46)$$

$$\hat{u}_{10} = \hat{w}_{5p} = \hat{w}_{10} = -\hat{n}_{10} = \hat{u}_{11} \quad (47)$$

$$\hat{n}_{11} = R_{\alpha_{10,11}} \hat{n}_{10} \quad (48)$$

$$\hat{v}_{11} = \text{Refract}[\hat{u}_{11}, \hat{n}_{11}, n_{\text{optic}}, n_{\text{vacuum}}] \quad (49)$$

The SRM wedge angle, $\alpha_{10,11}$, is determined by minimizing the z component of the output ray vector from the SRM:

$$\hat{w}_{11} \bullet \hat{k} \equiv 0 \quad (50)$$

Step 6) Having determined the PRM wedge angle for the non-folded IFO, it is used in the folded IFO. The ray vector through the PRM and into the BS as well as the ray vectors into each of the ITMs are known. In addition, the orientation of the BS for the folded IFO is defined to be the same as for the non-folded IFO (i.e. setting the normal vector \hat{n}_4 to be the same for both IFOs). The FM orientation is then determined by simultaneous solution of the following equations:

$$\hat{u}_{10} \bullet \hat{j} \equiv \hat{v}_9 \bullet \hat{j} = \text{Reflect}[\text{Reflect}[\hat{u}_4, \hat{n}_4], \hat{n}_9] \bullet \hat{j} \quad (51)$$

$$\hat{u}_{10} \bullet \hat{k} \equiv \hat{v}_9 \bullet \hat{k} = \text{Reflect}[\text{Reflect}[\hat{u}_4, \hat{n}_4], \hat{n}_9] \bullet \hat{k} \quad (52)$$

$$\hat{u}_7 \bullet \hat{i} \equiv \hat{v}_6 \bullet \hat{i} = \text{Reflect}[\text{Refract}[\text{Refract}[\hat{u}_4, \hat{n}_4, n_{\text{vacuum}}, n_{\text{optic}}], \hat{n}_5, n_{\text{optic}}, n_{\text{vacuum}}], \hat{n}_6] \bullet \hat{i} \quad (53)$$

$$\hat{u}_7 \bullet \hat{k} \equiv \hat{v}_6 \bullet \hat{k} = \text{Reflect}[\text{Refract}[\text{Refract}[\hat{u}_4, \hat{n}_4, n_{\text{vacuum}}, n_{\text{optic}}], \hat{n}_5, n_{\text{optic}}, n_{\text{vacuum}}], \hat{n}_6] \bullet \hat{k} \quad (54)$$

These 4 equations are used to define the orientation of FM_x , \hat{n}_9 , and FM_y , \hat{n}_6 .

The orientation of the surface normal vector, \hat{n}_{12} , and wedge angle, $\alpha_{12,13}$, for the SRM for the folded interferometer is determined in the same manner as for the non-folded interferometer.